Published in final edited form as:
Free Radic Biol Med. 2013 December ; 65: . doi:10.1016/j.freeradbiomed.2013.06.008.

Aldose reductase regulates acrolein-induced cytotoxicity in human small airway epithelial cells

Umesh CS Yadav, **KV Ramana**, and **SK Srivastava***
Department of Biochemistry and Molecular Biology, University of Texas Medical Branch, Galveston, Texas, 77555

Abstract

Aldose reductase (AR), a glucose metabolizing enzyme, reduces lipid aldehydes and their glutathione conjugates with more than 1000-fold efficiency (Km aldehydes 5-30μM) than glucose. Acrolein, a major endogenous lipid peroxidation product as well as component of environmental pollutant and cigarette smoke, is known to be involved in various pathologies including atherosclerosis, airway inflammation, COPD, and age-related disorders but the mechanism of acrolein-induced cytotoxicity is not clearly understood. We have investigated the role of AR in acrolein-induced cytotoxicity in primary human small airway epithelial cells SAECs. Exposure of SAECs to varying concentrations of acrolein caused cell-death in a concentration- and time-dependent manner. AR inhibition by fidarestat prevented the low (5 to 10 μM) but not high (>10 μM) concentrations of acrolein-induced SAECs cell death. AR inhibition protected SAECs from low dose (5 μM) acrolein-induced cellular reactive oxygen species (ROS). Inhibition of acrolein-induced apoptosis by fidarestat was confirmed by decreased condensation of nuclear chromatin, DNA fragmentation, comet tail-moment, and annexin-V fluorescence. Further, fidarestat inhibited acrolein-induced translocation of pro-apoptotic proteins Bax and Bad from cytosol to the mitochondria, and that of Bcl2 and Bcl_{XL} from mitochondria to cytosol. Acrolein-induced cytochrome c release from mitochondria was also prevented by AR inhibition. The mitogen-activated protein kinases (MAPK) such as extracellular signal-regulated kinases 1 and 2 (ERK1/2), stress-activated protein kinases/c-jun NH2-terminal kinases (SAPK/JNK) and p38MAPK, and c-jun were transiently activated in airway epithelial cells by acrolein in a concentration and time-dependent fashion, which were significantly prevented by AR inhibition. These results suggest that AR inhibitors could prevent acrolein-induced cytotoxicity in the lung epithelial cells.

Keywords

Aldose reductase; acrolein; apoptosis; cytotoxicity; COPD

*Corresponding Author: **Satish K Srivastava, Ph.D.** Professor Dept. of Biochemistry and Molecular Biology The University of Texas Medical Branch 6.644 Basic Science Building 301 University Blvd. Galveston, TX 77555-0647 Tel: (409)772-3926 Fax: (409)772-9679 ssrivast@utmb.edu.

Introduction

Acrolein is a ubiquitous environmental pollutant that arises from incomplete combustion of plastic materials, forest fires, cigarette smoke, and pyrolyzed animal and vegetable fats [1-3]. Presence of acrolein in the ambient air in urban atmosphere represents a considerable exposure hazard to human resulting in various health problems including atherosclerosis and airway disease such as asthma, chronic obstructive pulmonary disease (COPD), cystic fibrosis and carcinogenesis [2,4-8]. Along with the strong reactive aldehyde 4-hydroxy-2-nonenal (HNE), acrolein is also produced in-situ as the toxic by-product of oxidative stress-induced endogenous lipid peroxidation [9]. Among , α,β-unsaturated aldehydes, acrolein is considerably the strongest electrophile and readily reacts with nucleophilic reactive groups of bio-molecules including the sulfhydryl group of cysteine, imidazole group of histidine, and amino group of lysine resulting in the inactivation of the proteins [10].

A number of reports have described the damaging effects of acrolein on the airway ciliary movement [11], airway inflammation, and infiltration of monocytes, macrophages, and lymphocytes in the interstitium, mucous-cell metaplasia, and airway enlargement. Acrolein is known to cause apoptosis in number of cell types including keratinocytes, neutrophils and airway cells [12-14]. However, the biochemical and molecular mechanisms involved in the cellular toxicity are not clearly understood.

Apoptosis is a programmed cell death mechanism and is known to play an important role in the development as well as in maintaining tissue homeostasis [15]. Oxidant-induced apoptosis involves morphological and biochemical changes such as DNA fragmentation into 180–200 pb, externalization of phosphatidylserine and cellular fragmentation forming apoptotic bodies [16, 17]. Triggered by different kinds of stimuli, mitochondrial apoptosis pathway is thought to be regulated by antiapoptotic (Bcl_2 and $Bcl\text{-}_{XL}$) and proapoptotic (Bad and Bax) members of Bcl2 family of proteins, which modulate the release of proapoptotic molecules such as cytochrome (cyt) c [18]. Translocation of Bad to the mitochondrial membrane eliminates the inhibitory effects of Bcl2 on Bax. Bax then forms Bax-Bax dimmers, forming pores on the outer mitochondrial membrane, which may result in mitochondrial permeability transition leading to the release of proapoptogenic molecules including cyt c [19]. Cyt c interacts with apoptosis protease activating factor in the cytosol which leads to activation of caspases in a sequential manner. The activated effector caspases cleave many cellular proteins including poly(ADP-ribose) polymerase (PARP) and inhibitor of DNase. This leads to characteristic morphological changes in cells akin to apoptosis including chromatin condensation, nuclear membrane breakage, cell blebbing and formation of apoptotic bodies. Further, at the molecular level apoptosis is regulated by oxidative stress-mediated activation of several signaling intermediates including the redox sensitive stress kinases that activate transcription factors including nuclear factor – kappa B (NF-kB) and activator protein (AP) −1 [20]. The oxidative activation of Jun-N-terminal kinase (JNK) and mitogen-activated protein kinase (MAPK) phosphorylates and activates c-Jun, thereby activate AP-1 [21, 22]. AP-1, a redox-sensitive transcription factor and known to regulate transcription of a number of inflammatory genes, utilizes cysteiene residues as the redox switches [23]. Among other redox-sensitive targets, ROS directly activate certain protein tyrosine kinases, which then activate downstream signaling cascades [24]. Further, ROS also inactivate protein tyrosine phosphatases resulting in the persistent activation of tyrosine kinases [24, 25]. Thus, oxidative stress induced by acrolein may activate redox signaling pathways that lead to enhanced expression of pro-apoptotic proteins which could be responsible for acrolein-induced cell death [26].

We have shown that inhibitors of aldose reductase have anti-inflammatory and anti-oxidative properties [27,28]. Aldose reductase (AR) is a stress response protein and a

metabolic enzyme that is known to detoxify aldehydes besides reducing glucose to sorbitol in hyperglycemia. Increased AR expression and activity have been linked with pathological conditions where acrolein levels are known to be elevated e.g. cigarette smoke-exposure [29]. Although extensive literature on acrolein toxicity is available, the role of AR in acrolein-induced cytotoxicity remains controversial and at best unclear. Therefore, we investigated the modulatory role of AR on acrolein-induced cell death using primary human small airway epithelial cells (SAECs). Our hypothesis is that AR is the mediator of low dose acrolein-induced cytotoxicity and thus AR inhibition could prevent acrolein-induced inflammatory signals and apoptosis in airway cells.

Our results show that inhibition of AR by fidarestat prevents acrolein-induced increased ROS levels, nuclear condensation and DNA degradation, imbalance in the translocation of pro- and anti-apoptotic proteins, and phosphorylation and activation of stress kinases that lead to increase in SAEC apoptosis.

Material and Methods

Reagents

Small airway epithelial basal medium (SABM), small airway epithelial growth media (SAGM™) bulletkit; and Reagentpack™ containing Trypsin 0.025%/EDTA 0.01%, Trypsin neutralizing solution (TNS) and HEPES-buffered saline solution were purchased from Lonza Walkersvillle, Inc. (Walkersville, MD). AR inhibitor, fidarestat was obtained as gift from Sanwa Kagaku Kenkyyusho Co., Japan and Livwell, USA. Acrolein was purchased from Sigma-Aldrich (St Louise, MO). Antibodies against Bad, Bax, Bcl_2, BclXL, cytochrome c, glyceraldehydes 3-phospahte dehydrogensae (GAPDH), cytochrome c coxidase unit IV (COX IV), poly (ADP-ribose) polymerase (PARP) and caspase-3 and those against phospho-JNK, -ERK1/2, -p38, -c-jun and JNK, ERK1/2, p38, c-jun were obtained from Cell Signaling Technology (Danvers, MA). Dihydroethidium (DHE) fluorescent dye was purchased from Molecular Probes, Invitrogen (Carlsbad, CA). The CometAssay™kit was purchased from Trevigen, Inc. (Gaithersburg, MD). The reagents and supplies used in the Western blot analysis were obtained from BioRad (Hercules, CA). All other reagents used were of analytical grade.

Cell Culture

Primary human Small Airway Epithelial Cells (SAECs) were obtained from Lonza Walkersville, Inc. (Walkersville, MD). The cells were cultured at 37°C in humidified atmosphere containing 95% air and 5% CO_2 according to the supplier's instructions and used between passages 3 and 6. The cells were cultured in small airway epithelial basal medium (SABM) as described [30].

MTT assay

The SAECs were plated in a 96-well plate at the density of 5000 cells/well and growth-arrested for 24 h by replacing complete medium with fresh basal medium containing AR inhibitor, fidarestat (10 μM) or carrier (PBS). The cells were incubated with various concentrations of acrolein (0, 5, 10, 15 and 20 μM) for 48 h or with 5μM of acrolein for various time points (0, 12, 24, 48 and 72h) unless otherwise indicated. At the end of incubation 10 μl of MTT (5 mg/ml) were added to each well and incubated at 37°C for 2 h. The medium was removed and 100% DMSO was added to each well to dissolve the formazan granules. Absorbance was measured at 570 nm using a 96-well plate reader. Results are expressed as mean absorbance ± SD (n=4).

Detection of ROS

Approximately 1×10^5 SAECs were seeded on chambered slides and starved in serum-free SABM with or without fidarestat for 24 h. The cells were washed with HBSS and treated with acrolein (5μM) for 2 h. SAEC were rinsed with HBSS and incubated with DHE (2.5 μM) at 37°C for 15 minutes. Subsequently the cells were rinsed in PBS and mounted with DAPI containing mounting medium (Vector Laboratories Inc., Burlingame, CA). The cells were observed and photomicrographs were acquired with an Olympus camera fitted on epifluorescence microscope with a 585 nm long-pass filter. The red fluorescence, indicative of superoxide in the cells, was quantified using AlphaEaseFC software of AlphaImager 2200 (Alpha Innotech Corp.; Randburg, South Affrica) and shown as bar diagram (n=3). The DAPI staining was used to depict cell nucleus, which appear blue.

Determination of apoptosis by nuclear condensation assay

The SAECs were grown to 75-80% confluency in 2-chambered slides and growth-arrested in 0.1% serum medium without or with AR inhibitor, fidarestat. After 24 h, acrolein (5μM) without or with fidarestat were added to the basal media and the cells were incubated for another 24 h. At the end of incubation, the cells were washed with cold HBSS and mounted with mounting medium containing DAPI (Vector Laboratories Inc., Burlingame, CA). The cells were subsequently observed and photomicrographs were acquired with an Olympus camera fitted on epifluorescence microscope. The cells with fragmented and/or condensed nuclei were classified as apoptotic cells and quantified by manual counting per viewing area. The mean values ± SD from each group (n=3) are presented as bar diagram.

Determination of DNA damage

The comet assay was performed essentially as described in suppliers (Trevigen, Inc. Gaithersburg, MD) manual under dark (with no lights) condition as described by us earlier [31]. Briefly, 2×10^5 SAECs were plated in a 6-well plate, and starved in 0.1% serum medium without or with fidarestat (10 μM) for overnight. The cells were washed with HBSS and stimulated with acrolein (5 μM) for 3 h. Subsequently, the cells were harvested and centrifuged at 500xg for 5 min at room temperature. Supernatant was discarded and the cells in the pellets were re-suspended in PBS and were mixed with 1% low melting point (LMP) Agarose in 1:10 ratio. Immediately, 75 μl of the cell suspension was pipetted and dispersed onto CometSlides. The slides were placed at 4 °C in dark for 30 min to solidify Agarose and subsequently immersed in a lysis solution (10 mM Tris–HCl, 100 mM EDTA (pH 10), 2.5 M NaCl, 1% sodium lauryl sarcosinate, 1% Triton X-100,) for 60 min. The slides were washed with 1×Tris-buffered EDTA (TBE) solution. The electrophoresis was carried out in a horizontal electrophoresis chamber at the rate of 1.0 volt/cm for 20 min. Subsequently, the slides were washed in deionized water, dipped in 70% alcohol, air dried, and stained with SYBR-Green. The comet images were obtained using epifluorescence (epi800) microscope and at least 40 comets per slide were observed and quantified (% DNA in tail) using image analysis software, Comet Score™(TriTek Corp., Sumerduck, VA).

For DNA laddering assay, the confluent SAECs in T-75 flasks were starved overnight in the presence or absence of fidarestat for overnight, washed twice with HBSS and exposed to acrolein (5 μM) for 18 h without or with fidarestat (10 μM). The cells were harvested, washed with ice-cold PBS, and DNA was extracted using DNeasy Kit (Qiagen Inc., Valencia, CA) according to manufacturer's protocol using RNase to digest RNA. The extracted DNA (1μg) was subjected to electrophoresis on 1.5% Agarose gel containing ethidium bromide. UV-irradiated A549 cells-derived DNA was used as positive control. After electrophoresis, DNA fragments were visualized and images were captured by biospectrum 410 image systems from Ultra Violate Products Ltd. (Cambridge, UK).

Cell Cycle analysis

The SAECs were grown to confluence in a T-75cm^2 flasks and growth-arrested for 24 hours by replacing fresh medium containing 0.1% FBS and AR inhibitor fidarestat (10 μM), or carrier (PBS). After 24 hours, the cells were washed with HBSS and incubated with acrolein (5μM) in basal medium without or with fidarestat and the cells were incubated for an additional 24 h. The cells were harvested, washed, and fixed in 70% chilled ethanol for 2 hours followed by staining with propidium iodide (50μg/mL) in FACS buffer for 20 minutes. The Cell cycle analysis was performed by flow cytometry (FACSCanto; BD Biosciences, San Jose, CA).

AR siRNA transfection

The SAECs were seeded (2×10^5cells/well) in 6-well plate and incubated overnight. The AR siRNA transfection was performed by incubating the cells in basal media containing human AR-siRNA (AACGCAUUGCUGAGAACUUUAUU) to a final concentration of 20 nM and the hIpERfECT transfection reagent (Qiagen Inc., Valencia, CA) as described by the supplier. Briefly, 700 ng AR siRNA per well was diluted in 100 μl serum-free medium and subsequently mixed with 18 μl HiPerFect transfection reagent and incubated for 10 min at room temperature. The transfection mixture was then added to the respective wells containing 700 μl complete culture media and incubated for 3 h at 37°C. Subsequently, 1.6 ml complete culture medium was added to each well and cells were incubated for 24 h. One group of cells was trypsinized and plated in 96-well plate for MTT assay as described above. In the other group incubated for 48 h post transfection, changes in the expression of AR were assessed by Western blot analysis using anti-AR antibodies.

Annexin V FITC assay

The SAECs (5000 cells/well) were seeded in a 96-well plate grown till 80% confluence. The growth-arrested cells without or with fidarestat (10 μM) were incubated with acrolein (5 μM) for 8 h at 37°C. At the end of incubation the cells were stained with annexin V FITC following manufacturers protocol (Cayman Chemical, Ann Arbor, MI) and the fluorescence was detected with excitation and emission wavelengths of 485 and 535 nm, respectively using a 96-well plate reader (Biotek, Winooski, VT). Results are expressed as mean fluorescence +/− SD (n=4).

Preparation of cytosolic and mitochondrial fraction

The mitochondrial and cytosolic fractions of the SAECs were prepared using the cytochrome c assay kit from Abcam (Cambridge, MA). Briefly, the cells were harvested and washed with ice-cold PBS and resuspended in cytosol extraction buffer mix and incubated on ice for 10 mins. The cells were homogenized using Dounce homogenizer and centrifuged for 10 mins at 700xg and the supernatant was further centrifuged at 10,000xg for 30 min at 4°C. At this stage, supernatant was collected and labeled as cytosolic fraction. The pellet was suspended in mitochondrial extraction buffer, mixed by vortexing and labeled as mitochondrial faction. Both cytosolic and mitochondrial factions were used to determine the translocation and release of Bcl_2 member proteins and cytochrome c, respectively by Western blotting as described below.

Western blot analysis

The whole cell lysates were prepared using RIPA lysis buffer and equal amount of proteins (40 μg) were resolved on 10% SDS-PAGE. The proteins were transferred to a nitrocellulose membrane using Trans-Blot turbo transfer system from BioRad (Hercules, CA). The membranes were blocked with 5% nonfat milk in Tris-Buffered Saline Tween-20 (TBST) and probed with primary antibodies (1:1,000 dilutions) for 3 h at room temperature or

overnight at 4°C. The blots were washed with TBST for 3 times, 5 min each, and exposed to HRP-conjugated secondary antibodies (1:5,000 dilution) for 1 h and the antigen-antibody complex was detected by enhanced chemiluminescence (Amersham Pharmacia Biotech, Piscataway, NJ). The immune-positive bands were quantified by scanning and determining the pixel density by using AlphaEaseFC software of AlphaImager 2200 (Alpha Innotech Corp.; Randburg, South Affrica).

Statistical analysis

The data presented are mean ± SD and P values were determined by unpaired, two-tailed Student's t test using Graph-pad prism software. $p<0.05$ was considered as statistically significant.

Results

Effect of AR inhibition on acrolein-induced cell death in SAECs

We first investigated the role of AR in acrolein-induced cellular toxicity in SAEC. The airway epithelial cells abundantly express AR and treatment with fidarestat for 24 h significantly inhibited AR activity as well as expression (data not shown). The dose and time-dependent decrease in the cell viability in SAECs by low doses of acrolein (<10μM) was significantly prevented by AR inhibition (Fig 1A, and B). However, the decrease in the cell viability of SAECs at doses of acrolein (>10μM) was not prevented by AR inhibition (Fig 1A) indicating that AR inhibition offers protection at lower acrolein doses while remains ineffective at higher doses. To further confirm the involvement of AR in low dose acrolein-induced cytotoxicity, we performed loss of function studies using AR siRNA in SAECs. As shown in Fig 1C, Acrolein-induced loss of cell's viability in SAECs was prevented in AR-ablated cells, indicating the role of AR in acrolein cytotoxicity.

Effects of AR inhibition on acrolein-induced ROS generation in SAECs

The cellular toxicity and DNA damage are indicative of increased oxidative stress in cells upon exposure to acrolein [16]. To investigate the role of acrolein-induced oxidative stress in the cellular apoptosis, we determined ROS levels in SAECs subsequent to acrolein exposure in the absence and presence of fidarestat. As shown in Fig 2 incubation with acrolein caused a significant (~3.5-fold) increase in intracellular ROS levels, as indicated by red fluoresce around the nuclei in acrolein treated cells (Fig 2A), which was significantly (by >50%) prevented in fidarestat treated and acrolein exposed SAECs (Fig 2B). These results indicate that acrolein-induced ROS generation could be prevented by AR inhibition, which plays a protective role in acrolein-induced airway epithelial cell damage.

Effect of AR inhibition on the acrolein-induced translocation of apoptotic proteins

Cellular apoptosis is mediated by a fine balance of pro- and anti-apoptotic proteins in cells. Specifically, mitochondrial apoptosis pathway is regulated by early translocation of antiapoptotic (Bcl_2 and $Bcl\text{-}_{XL}$) and proapoptotic (Bad and Bax) members of Bcl2 family proteins to or from mitochondria [18], which modulate the release of proapoptotic molecules such as cyt c that activates the effecter caspases and DNases. We therefore, investigated in SAECs the translocation of Bcl_2 member proteins to mitochondria or cytosol following incubation with acrolein in the absence or presence of fidarestat. As shown in Fig 3, acrolein caused translocation of proapoptotic members such as Bad and Bax to the mitochondria, while that of anti-apoptotic members to the cytosol. These changes were significantly prevented in fidarestat-treated SAECs followed by acrolein exposure. Further, the release of proapoptotic molecule cyt c was more in the cytosolic fraction indicating its release from mitochondria subsequent to acrolein exposure, which was inhibited in the cells treated with

AR inhibitor, fidarestat. These results indicate that low-dose acrolein activates mitochondrial apoptotic pathway and AR inhibition prevents it.

Effects of AR inhibition on acrolein-induced DNA damage and nuclear condensation

Since aldehyde-induced cytotoxicity is known to be caused by oxidative damages to DNA [31], we next examined the effect of AR inhibition on acrolein-induced DNA damage in SAECs using comet and DNA-laddering assays. As shown in Fig 4A, the comet tails were visible in acrolein treated cells as compared to the control cells. Upon quantification, the comet tail intensity (% DNA in comet tail) in acrolein-treated cells was significantly elevated and in AR inhibitor-treated group, these parameters were significantly low (Fig 4B). Similarly, acrolein -induced DNA damage in SAECs showed a characteristic ladder pattern, a characteristic of apoptosis, when subjected to agarose gel electrophoresis indicating apoptosis in those cells. The DNA ladder was absent in AR inhibitor-treated SAECs (Fig 4C). These results suggest that AR inhibition could protect SAECs from apoptosis caused by exposure to toxic aldehydes.

To further confirm that the nature of apoptotic cell death, we performed nuclear condensation assay. SAECs were incubated with acrolein (5 μM) for 18 h with or without fidarestat, and nuclear condensation was examined by fluorescent microscope following nuclear staining with 4',6-diamidino-2-phenylindole (DAPI). As shown in Fig 5A, there were numerous condensed and blebbed nuclei in acrolein-treated group (marked with arrow) as compared to acrolein + fidarestat-treated group. Further, as shown in Fig 5B, significantly increased number (~8- fold) of acrolein-treated cells showed nuclear condensation whereas in AR inhibitor-treated cells nuclear condensation was significantly (~50%) prevented. In order to affirm that the acrolein-induced cell death was indeed due to apoptosis, we performed Annexin V FITC staining to capture the early cell death, i.e. externalization of phosphatidylserine. A fluorochrome-labeled annexin V binds specifically to externalized phosphatidylserine in early apoptotic cells. This was detected by measuring the fluorescence in a plate reader. As shown in Fig 5C, there was significant increase in the annexin V-specific mean fluorescence intensity (MFI) in acrolein-exposed cells, which was significantly prevented in fidarestat-treated cells. Collectively, these data suggest that inhibition of AR prevents low dose acrolein-induced DNA damage and nuclear condensation, well known characteristics of apoptosis, which may be responsible for decreased cell death in fidarestat-treated cells.

Effect of AR inhibition on the acrolein-induced cell cycle changes in SAECs

ROS-induced cell cycle arrest in the G2 phase is known to lead to apoptosis [32]. Therefore, we examined the effect of AR inhibition on acrolein-induced cell cycle arrest in SAECs. The serum-starved quiescent cells were exposed to acrolein (5 μM) for 24 h with or without fidarestat following which the cells were harvested and subjected to FACS analysis. As shown in Fig 6A, significantly (~3-fold) increased numbers of nuclei with double set of DNA (27.9%) were observed in post synthetic G2 phase of cell cycle in acrolein-treated group as compared to control (9.08%), suggesting a G2 arrest. Similarly, as shown in Fig 6B, increased number of cells were found in acrolein-treated group. On the other hand treatment with fidarestat significantly decreased these numbers indicating the protection from acrolein-induced cytotoxicity.

Effect of AR inhibition on the acrolein-induced activation of stress kinases

Since stress kinases such as MAKP, SAPK/JNK and c-Jun that activate redox sensitive transcription factors play important role in apoptosis [21, 22], we next examined the phosphorylation and activation of these proteins. As shown in Fig 7, acrolein caused dose-dependent increase in the phosphorylation of JNK, while ERK1/2 and p38 showed increased

phosphorylation on lower doses of 1 and 5 μM only. In the fidarestat-treated cells, on the other hand, a marked decrease in acrolein-induced phosphorylation of these kinases was observed as compared to the un-phosphorylated form of these proteins, which remained mostly unaltered. Similarly, when airway epithelial cells were stimulated with 5 μM of acrolein for different time points, a rapid increase in the phosphorylation of ERK1/2 and JNK MAP kinases within 5 to 15 min was observed, which decreased significantly in AR inhibitor treated cells (Fig 8).

We next investigated phosphorylation of c-jun, a subunit of redox-sensitive transcription factors AP-1, by acrolein. A low dose acrolein exposure of SAECs caused a dose-dependent (Fig 7 lowest panel) as well as a time-dependent (Fig 8, lowest panel) increase in the phosphorylation of c-jun, indicating the activation of transcription factor AP-1. In the presence of AR inhibitor, acrolein-induced phosphorylation of c-jun decreased significantly (Figs 7, 8).

Taken together, these results indicate a dose- and time-dependent increase in the phosphorylation and activation of redox-sensitive signaling kinases and transcription factors, known to regulate oxidative stress-induced cytotoxicity and AR inhibition prevented these changes suggesting that AR regulates low-dose acrolein-induced changes in cell physiology that cause programmed cell-death by activating redox-sensitive signaling molecules.

Discussion

A number of studies suggest that acrolein-induced toxic effects are due to its conjugation with cellular GSH, resulting in the formation of GS-acrolein conjugate thereby depleting cellular GSH [33, 34]. This reaction is catalyzed by glutathione-S-transferase (GST), but could also occur spontaneously due to high electrophilic nature of acrolein [34]. Depletion of GSH results in increased oxidative stress that causes cytotoxicity. The increase in oxidative stress causes endogenous activation of lipid peroxidation pathway, which produces more lipid aldehydes such as acrlein and further accentuates the stress. Aldehydes are known to cause cell death by apoptosis as well as necrosis depending upon their concentration [35]. At the lower concentration (<5μM), aldehydes cause GSH depletion which results in increased cellular ROS levels followed by increase in inflammatory markers leading to apoptosis [36, 37]. Simultaneously, cells try to circumvent these effects by enhancing antioxidant machinery including induction of antioxidant enzymes [38]. Acrolein is known to cause oxidative stress by inducing, directly or indirectly, the production of excessive ROS which promotes to cellular apoptosis [35, 39, 40]. In the present study, increase in the cytotoxicity of airway epithelial cells subsequent to acrolein exposure shows concurrence with previous findings. Additionally, cells showed significantly increased levels of ROS after acrolein exposure, which correlated with acrolein-induced apoptosis in airway epithelial cells. However, when treated with fidarestat, the ROS level as well as apoptotic cell death decreased in SAECs, indicating protective role of AR inhibition in low-dose acrolein-induced lung epithelial cells cytotoxicity. Further, acrolein has been shown to cause DNA damage in many cells, which is linked with apoptosis [4, 16]. Consistent with these studies we also observed that acrolein-treated cells had significantly more DNA degradation and DNA strand-breaks compared to the control cells. Our findings in the present study suggest that inhibition of AR prevents acrolein-induced DNA strand-breaks and degradation, thereby protects from acrolein-induced cytotoxicity.

In order to investigate the effect of AR inhibition of the early apoptotic events, we examined the translocation of Bcl2 family proteins in cells. Mitochondrial apoptosis pathway is known to be regulated by members of Bcl2 family proteins which include antiapoptotic (Bcl_2 and $Bcl\text{-}_{XL}$) and proapoptotic (Bad and Bax) members [18]. Stimulated by the oxidants such as

acrolein, Bad translocates to the mitochondria and removes the inhibitory effects of Bcl2 on the Bax, which leads to formation of Bax-Bax dimmer pores on the outer membrane that could alter mitochondrial permeability. This results in the release of proapoptotic molecules such as cyt c. It has been shown that changes in mitochondrial permeability leads to the release of cytochrome *c* from mitochondria, which is required for the hallmarks of cytosolic and nuclear apoptosis such as caspase 3 activation and nuclear laddering [19]. The present study provides new information on the role of AR in the regulation of mitochondrial pathway of acrolein-induced apoptosis and results suggest that inhibition of AR prevents translocation of pro-apoptotic proteins Bax and Bad to the mitochondria and that of Bcl2 from mitochondria to cytosol. Further, once in cytosol, cyt c activates caspases which cleave many cellular proteins including poly(ADP-ribose) polymerase (PARP) and inhibitor of DNase leading to apoptosis which is marked by DNA damage, chromatin condensation, nuclear membrane breakage, cell blebbing and formation of apoptotic bodies. We have demonstrated in this study that acrolein-induced cyt c release into cytosol was inhibited by AR inhibition, which may lead to the inhibition of PARP-1 cleavage, DNA strand break, nuclear condensation and eventually of apoptosis. The effect of AR inhibition on the acrolein-induced cytotoxicity of the airway epithelial cells was further evident by inhibition of acrolein-induced cell cycle arrest in AR inhibitor-treated cells.

Increased level of oxidative stress causes activation of redox signaling via phosphorylation and activation of redox-sensitive kinases such as MAPK, SAPK/JNK and transcription factors c-jun [20-22,41]. Further, treatment with acrolein has been shown to increase phosphorylation of ERK1/2, p38, and JNK in human umbilical vein endothelial cells leading to activation and nuclear translocation of the redox-sensitive transcription factor NF-kB and subsequent increase in inflammatory cytokines and chemokines including TNF-α, IL-6 and IL-8 [42]. We therefore, examined the phosphorylation of various kinases including p38, SAPK/JNK and c-jun in response to acrolein. Our results indicate that low dose acrolein induces a redox imbalance and activates the stress kinases which lead to the activation of c-jun, a constituent of transcription factor AP-1. Since AP-1 is known to transcribe inflammatory markers that cause cytotoxicity, our findings suggest that AR inhibition may prevent acrolein-induced activation of signaling cascade that cause cellular toxicity via expression of inflammatory markers. We have shown previously that AR inhibition prevents HNE-induced expression of inflammatory markers iNOS and COX-2 in macrophages [43].

Although the precise mechanism of how AR induces aldehydes-mediated apoptosis is not known, we contemplate that metabolic product of glutathione-acrolein conjugates catalyzed by AR could be involved in the activation of ROS-mediated signaling intermediates. Inhibition of AR may prevent apoptosis by blocking the activation of redox-sensitive signaling cascade in addition to inhibiting the translocation of Bcl_2 family member proteins as evident by present findings (Fig 9) [27,28]. We have previously demonstrated similar phenomenon in mouse macrophages where AR inhibitors prevented HNE and GS-HNE-induced cytotoxic effects but not that induced by GS-DHN [43]. These observations bequeath an important role to AR-catalyzed reduced product of glutathione-acrolein conjugate in the aldehydes-induced cytotoxicity and indicate that AR inhibition could play a protective role in low-dose aldehyde exposure-related injury. Indeed, GS-acrolein has been found to be more nephrotoxic than acrolein alone [44]. It has been reported previously that down regulation of AR renders the macrophages susceptible to acrolein-induced cell death, which is in contrast with our finding [45]. Besides the difference in the cell type (macrophages vs airway epithelial cells) and their source (cell line vs primary cells), another reason behind this difference in observation could be the higher concentration (25 μM) of acrolein used in that study in compared to a lower concentration of 5 μM used in the present study. However, we also observed that at higher concentration of acrolein, the cell death was not prevented by AR inhibition, suggesting that higher aldehyde concentrations overwhelms

the cellular antioxidant and protection machinery and cells could undergo direct necrosis than apoptosis. Nevertheless, these differences need to be taken in consideration for mechanistic studies in future.

Taken together, our results provide evidence that AR inhibition prevents low dose acrolein-induced sub-cellular translocation of apoptogenic Bcl2 family proteins and modulates cytotoxic signals by inhibiting the activation of ROS formation and subsequent activation of inflammatory signals in airway epithelial cells.

Acknowledgments

This study was supported by American Asthma Foundation grant (AAF 08-0219) and National Institutes of Health (NIH) Grant DK36118 to SKS. This study was also supported by NIEHS core facility grant (ES00667616A1).

References

1. World Health Organization (WHO) Geneva. Acrolein, IPCS International programme on chemical safety, Concise International Chemical Assessment Document. 2002; 43
2. Beauchamp RO Jr. Andjelkovich DA, Kligerman AD, Morgan KT, Heck HD. A critical review of the literature on acrolein toxicity. Crit. Rev Toxicol. 1985; 14:309–380. [PubMed: 3902372]
3. Johnstone RAW, Plimmer JR. The Chemical Constituents of Tobacco and Tobacco Smoke. Chem. Rev. 1959; 59:885–936.
4. Feng Z, Hu W, Hu Y, Tang MS. Acrolein is a major cigarette-related lung cancer agent: preferential binding at p53 mutational hotspots and inhibition of DNA repair. Proc. Natl. Acad. Sci. U.S.A. 2006; 103:15404–15409. [PubMed: 17030796]
5. Samet JM, Cheng PW. The role of airway mucus in pulmonary toxicology. Environ. Health Perspect. 1994; 102:89–103. [PubMed: 7925190]
6. Hogg JC. Chronic obstructive pulmonary disease: an overview of pathology and pathogenesis. Novartis Found. Symp. 2001; 234:4–19. [PubMed: 11199102]
7. Saetta M. Airway inflammation in chronic obstructive pulmonary disease. Am. J. Respir. Crit. Care Med. 1999; 160:S17–S20. [PubMed: 10556163]
8. Witschi H, Joad JP, Pinkerton KE. The toxicology of environmental tobacco smoke. Annu. Rev. Pharmacol. Toxicol. 1997; 37:29–52. [PubMed: 9131245]
9. Adams JD Jr. Klaidman LK. Acrolein-induced oxygen radical formation. Free Radic Biol Med. 1993; 15:187–193. [PubMed: 8397144]
10. Esterbauer H, Schaur RJ, Zollner H. Chemistry and biochemistry of 4-hydroxynonenal, malonaldehyde and related aldehydes. Free Radic Biol Med. 1991; 11:81–128. [PubMed: 1937131]
11. Kensler CJ, Battista SP. COMPONENTS OF CIGARETTE SMOKE WITH CILIARYDEPRESSANT ACTIVITY. THEIR SELECTIVE REMOVAL BY FILTERS CONTAINING ACTIVATED CHARCOAL GRANULES. N. Engl. J. Med. 1963; 269:1161–1166. [PubMed: 14061124]
12. Takeuchi K, Kato M, Suzuki H, Akhand AA, Wu J, Hossain K, Miyata T, Matsumoto Y, Nimura Y, Nakashima I. Acrolein induces activation of the epidermal growth factor receptor of human keratinocytes for cell death. J. Cell. Biochem. 2001; 81:679–88. [PubMed: 11329622]
13. Finkelstein EI, Nardini M, van der Vliet A. Inhibition of neutrophil apoptosis by acrolein: a mechanism of tobacco-related lung disease? Am. J. Physiol. Lung Cell. Mol. Physiol. 2001; 281:L732–739. [PubMed: 11504702]
14. Nardini M, Finkelstein EI, Reddy S, Valacchi G, Traber M, Cross CE, van der Vliet A. Acrolein-induced cytotoxicity in cultured human bronchial epithelial cells. Modulation by alpha-tocopherol and ascorbic acid. Toxicology. 2002; 170:173–185. [PubMed: 11788155]
15. Chandra J, Samali A, Orrenius S. Triggering and modulation of apoptosis by oxidative stress. Free Radic. Biol. Med. 2000; 29:323–333. [PubMed: 11035261]

16. Tang MS, Wang HT, Hu Y, Chen WS, Akao M, Feng Z, Hu W. Acrolein induced DNA damage, mutagenicity and effect on DNA repair. Mol Nutr Food Res. 2001; 55:1291–1300. [PubMed: 21714128]

17. Schwarz M, Andrade-Navarro MA, Gross A. Mitochondrial carriers and pores: key regulators of the mitochondrial apoptotic program? Apoptosis. 2007; 12:869–876. [PubMed: 17453157]

18. Antonsson B. Mitochondria and the Bcl-2 family proteins in apoptosis signaling pathways. Mol. Cell. Biochem. 2004; 256/257:141–155. [PubMed: 14977177]

19. Yang JC, Cortopassi GA. Induction of the mitochondrial permeability transition causes release of the apoptogenic factor cytochrome c. Free Radic Biol Med. 1998; 24:624–631. [PubMed: 9559874]

20. Kalariya NM, Ramana KV, Srivastava SK, van Kuijk FJ. Carotenoid derived aldehydes-induced oxidative stress causes apoptotic cell death in human retinal pigment epithelial cells. Exp Eye Res. 2008; 86:70–80. [PubMed: 17977529]

21. Yoshizumi M, Abe J, Haendeler J, Huang Q, Berk BC. Src and Cas mediate JNK activation but not ERK1/2 and p38 kinases by reactive oxygen species. J Biol Chem. 2000; 275:11706–11712. [PubMed: 10766791]

22. Humar M, Loop T, Schmidt R, Hoetzel A, Roesslein M, Andriopoulos N, Pahl HL, Geiger KK, Pannen BH. The mitogen-activated protein kinase p38 regulates activator protein 1 by direct phosphorylation of c-Jun. Int J Biochem Cell Biol. 2002; 39:2278–2288. [PubMed: 17689131]

23. Karin M, Liu Zg. Zandi E. AP-1 function and regulation. Curr Opin Cell Biol. 1997; 9:240–246. [PubMed: 9069263]

24. Goldman R, Ferber E, Zor U. Involvement of reactive oxygen species in phospholipase A2 activation: inhibition of protein tyrosine phosphatases and activation of protein kinases. Adv Exp Med Biol. 1997; 400A:25–30. [PubMed: 9547533]

25. Dröge W. Free radicals in the physiological control of cell function. Physiol Rev. 2002; 82:47–95. [PubMed: 11773609]

26. Dang TN, Arseneault M, Ramassamy C. Regulation of redox-sensitive signaling pathways in rat primary astrocytes following acrolein exposure. J Alzheimers Dis. 2011; 25:263–277. [PubMed: 21422526]

27. Srivastava SK, Yadav UC, Reddy AB, Saxena A, Tammali R, Shoeb M, Ansari NH, Bhatnagar A, Petrash MJ, Srivastava S, Ramana KV. Aldose reductase inhibition suppresses oxidative stress-induced inflammatory disorders. Chem Biol Interact. 2011; 191:330–338. [PubMed: 21354119]

28. Srivastava SK, Ramana KV, Bhatnagar A. Role of aldose reductase and oxidative damage in diabetes and the consequent potential for therapeutic options. Endocr Rev. 2005; 26:380–392. [PubMed: 15814847]

29. Steiling K, Lenburg ME, Spira A. Airway gene expression in chronic obstructive pulmonary disease. Proc Am Thorac Soc. 2009; 6:697–700. [PubMed: 20008878]

30. Yadav UC, Ramana KV, Aguilera-Aguirre L, Boldogh I, Boulares HA, Srivastava SK. Inhibition of aldose reductase prevents experimental allergic airway inflammation in mice. PLoS One. 2009; 4:e6535. [PubMed: 19657391]

31. Yadav UC, Ramana KV, Awasthi YC, Srivastava SK. Glutathione level regulates HNE-induced genotoxicity in human erythroleukemia cells. Toxicol Appl Pharmacol. 2008; 227:257–264. [PubMed: 18096195]

32. Zhang L, Ruan J, Yan L, Li W, Wu Y, Tao L, Zhang F, Zheng S, Wang A, Lu Y. Xanthatin induces cell cycle arrest at G2/M checkpoint and apoptosis via disrupting NF-κB pathway in A549 non-small-cell lung cancer cells. Molecules. 2012; 17(4):3736–3750. [PubMed: 22450683]

33. Krokan H, Grafstrom RC, Sundqvist K, Esterbauer H, Harris CC. Cytotoxicity, thiol depletion and inhibition of O6-methylguanine-DNA methyltransferase by various aldehydes in cultured human bronchial fibroblasts. Carcinogenesis. 1985; 6:1755–1759. [PubMed: 4064250]

34. He NG, Awasthi S, Singhal SS, Trent MB, Boor PJ. The role of glutathione S-transferases as a defense against reactive electrophiles in the blood vessel wall. Toxicol Appl Pharmacol. 1998; 152:83–89. [PubMed: 9772203]

35. Mohammad MK, Avila D, Zhang J, Barve S, Arteel G, McClain C, Joshi-Barve S. Acrolein cytotoxicity in hepatocytes involves endoplasmic reticulum stress, mitochondrial dysfunction and oxidative stress. Toxicol Appl Pharmacol. 2012; 265:73–82. [PubMed: 23026831]
36. Aoshiba K, Yasui S, Nishimura K, Nagai A. Thiol depletion induces apoptosis in cultured lung fibroblasts. Am. J. Respir. Cell. Mol. Biol. 1999; 21:54–64. [PubMed: 10385593]
37. Kwolek-Mirek M, Bednarska S, Bartosz G, Biliński T. Acrolein toxicity involves oxidative stress caused by glutathione depletion in the yeast Saccharomyces cerevisiae. Cell Biol Toxicol. 2009; 25:363–378. [PubMed: 18563599]
38. Tirumalai R, Rajesh Kumar T, Mai KH, Biswal S. Acrolein causes transcriptional induction of phase II genes by activation of Nrf2 in human lung type II epithelial (A549) cells. Toxicol. Lett. 2002; 132:27–36. [PubMed: 12084617]
39. Luo J, Robinson JP, Shi R. Acrolein-induced cell death in PC12 cells: role of mitochondria-mediated oxidative stress. Neurochem Int. 2005; 47:449–57. [PubMed: 16140421]
40. O'Toole TE, Zheng YT, Hellmann J, Conklin DJ, Barski O, Bhatnagar A. Acrolein activates matrix metalloproteinases by increasing reactive oxygen species in macrophages. Toxicol Appl Pharmacol. 2009; 236:194–201. [PubMed: 19371603]
41. Ranganna K, Yousefipour Z, Nasif R, Yatsu FM, Milton SG, Hayes BE. Acrolein activates mitogen-activated protein kinase signal transduction pathways in rat vascular smooth muscle cells. Mol Cell Biochem. 2002; 240:83–98. [PubMed: 12487375]
42. Haberzettl P, Vladykovskaya E, Srivastava S, Bhatnagar A. Role of endoplasmic reticulum stress in acrolein-induced endothelial activation. Toxicol. Appl. Pharmacol. 2009; 234:14–24. [PubMed: 18951912]
43. Ramana KV, Fadl AA, Tammali R, Reddy AB, Chopra AK, Srivastava SK. Aldose reductase mediates the lipopolysaccharide-induced release of inflammatory mediators in RAW264.7 murine macrophages. J Biol Chem. 2006; 281:33019–33029. [PubMed: 16956889]
44. Horvath JJ, Witmer CM, Witz G. Nephrotoxicity of the 1:1 acrolein-glutathione adduct in the rat. Toxicol Appl Pharmacol. 1992; 117:200–207. [PubMed: 1471152]
45. Kang ES, Kim GH, Woo IS, Kim HJ, Eun SY, Ham SA, Jin H, Kim MY, Park MH, Kim HJ, Chang KC, Lee JH, Kim JH, Yabe-Nishimura C, Seo HG. Down-regulation of aldose reductase renders J774A.1 cells more susceptible to acrolein- or hydrogen peroxide-induced cell death. Free Radic Res. 2008; 42:930–938. [PubMed: 19031314]

Highlights

1. Aldose reductase (AR) mediates low-dose acrolein-induced cytotoxicity in airway epithelial cells
2. AR inhibition prevents acrolein-induced ROS formation and subsequent apoptosis
3. AR inhibition regulates cellular translocation of the Bcl2 family proteins and activation of effecter molecules
4. Acrolein-induced phosphorylation and activation of stress kinases in lung epithelial cells is prevented by inhibition of AR
5. AR inhibitors may be used to prevent acrolein-induced cytotoxicity in the lungs of acrolein-exposed subjects.

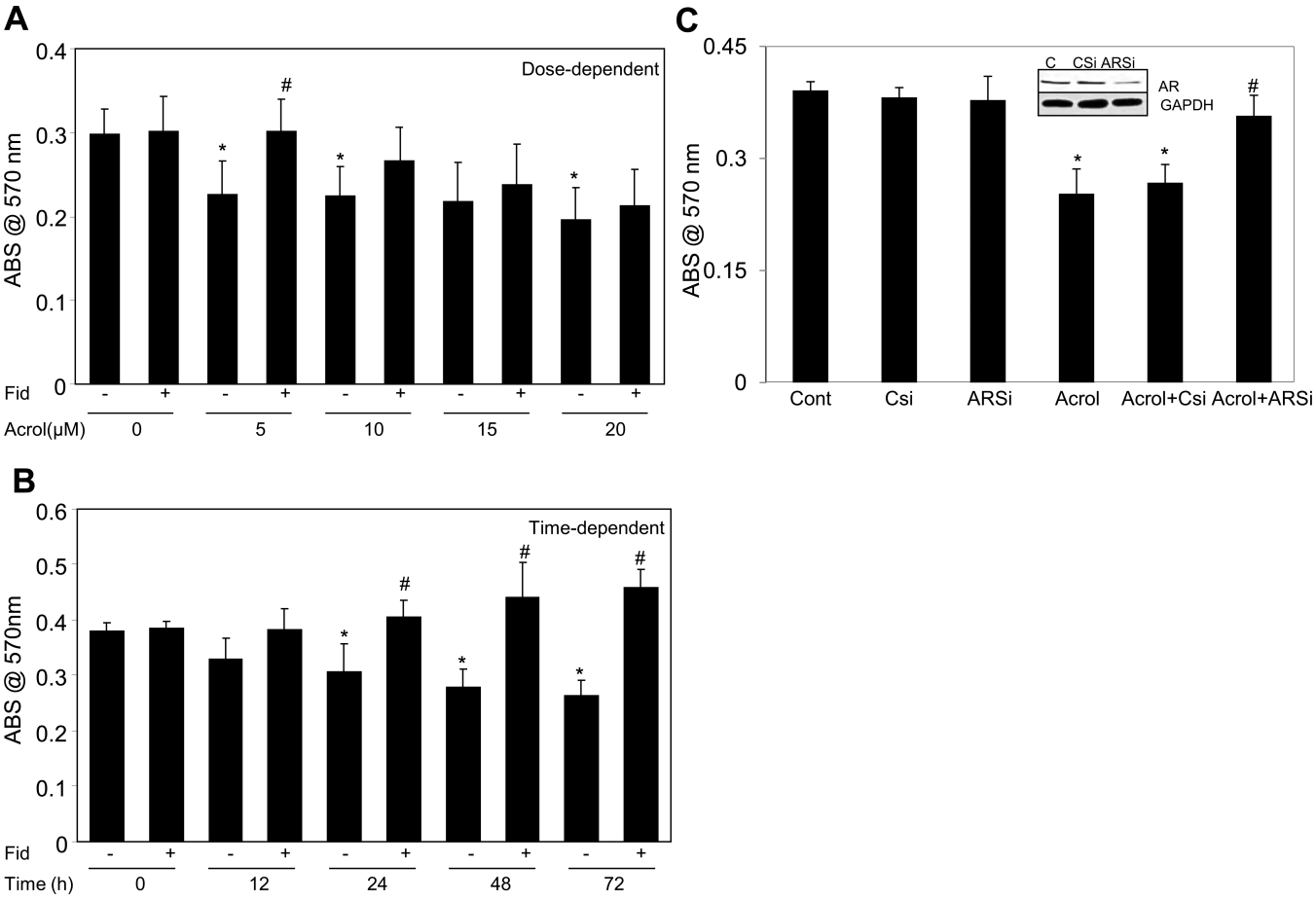

Fig 1. AR inhibition or siRNA ablation prevents acrolein-induced cell death in SAECs

In (A) and (B) the SAECs were seeded while in (C) the normal and siRNA transfected cells were seeded in a 96-well plate (5000 cells/well) and incuabted for overnight. The cells were starved for 24 h by incubating in 0.1% serum medium without or with AR inhibitor, fidarestat (10 μM) or carrier (PBS) as indicated. The cells were washed with HBSS and incubated with **(A)** different concentrations (0, 5, 10, 15 and 20 μM) of acrolein for 48 h; **(B)** with 5μM of acrolein for various time points (0, 12, 24, 48 and 72h) or **(C)** with 5μM of acrolein for 24 h. At the end of various incubations MTT assay was performed and absorbance at 570 nm is expressed as bars (mean±SD (n=4). *p<0.01 Vs Control; $^{\#}p$<0.05 Vs Acrolein alone. C, control; Fid, fidarestat; Acrol, acrolein; AR, aldose reductase; ARSi, aldose reductase specific siRNA

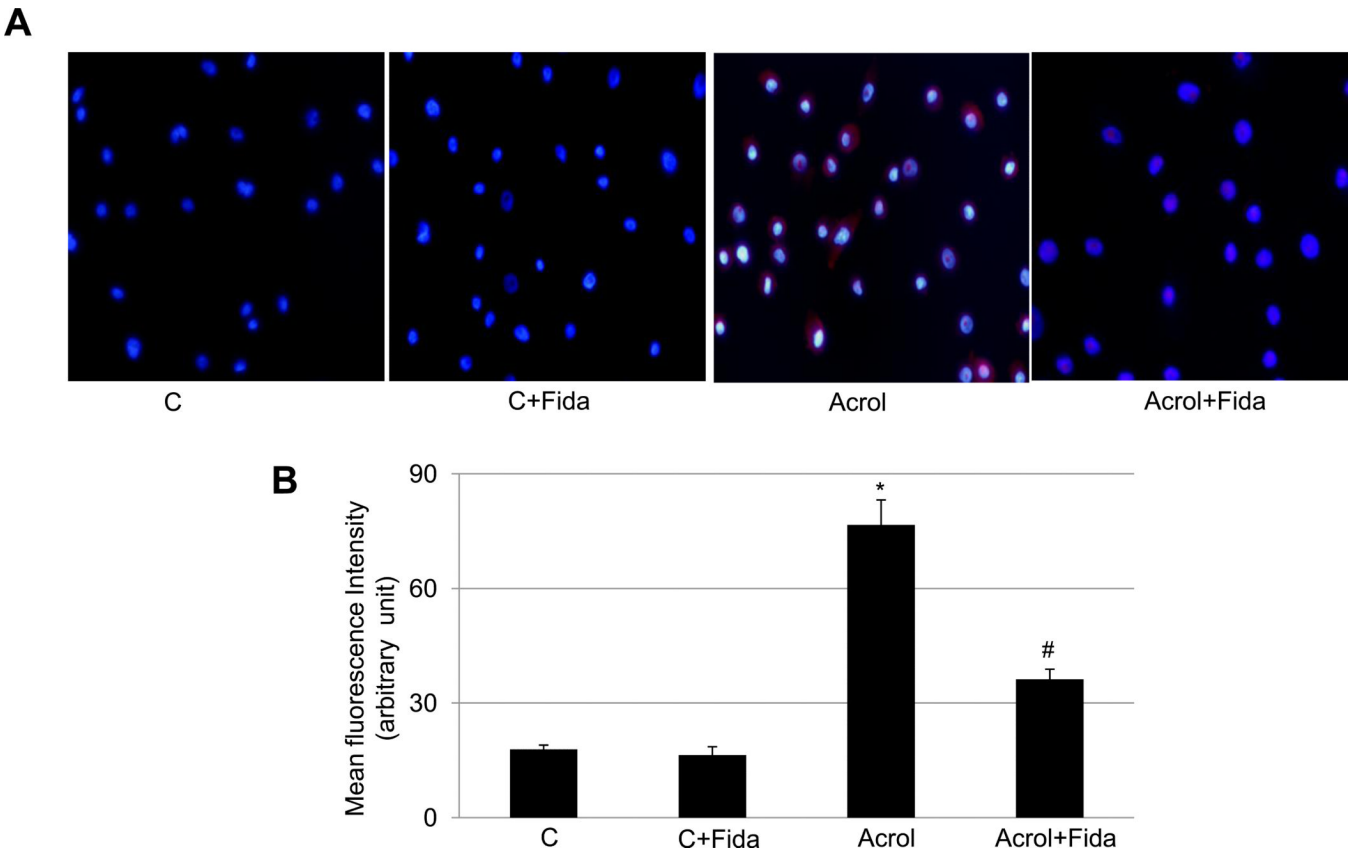

Fig 2. Effect of AR inhibition on Acrolein-induced ROS formation in SAECs

(A) Approximately 1×10^5 SAECs were seeded on 2-chambered slides and starved in serum-free SABM with or without fidarestat (10μM) for 24 h. The cells were washed with HBSS and treated with acrolein (5μM) for 2 h. SAEC were rinsed with HBSS and incubated with DHE (2.5 μM) at 37°C for 15 minutes. The cells were washed with PBS and mounted with DAPI containing mounting medium and observed with epifluorescence microscope. The representative photomicrographs are shown (n=3). **(B)** Quantification of DHE-specific red fluorescence, indicative of superoxide in the cells, is shown as bars (Mean±SD; n=3). *p<0.001 Vs Control; $^{\#}p$<0.05 Vs Acrolein. C, control; Acrol, Acrolein; Fida, fidarestat.

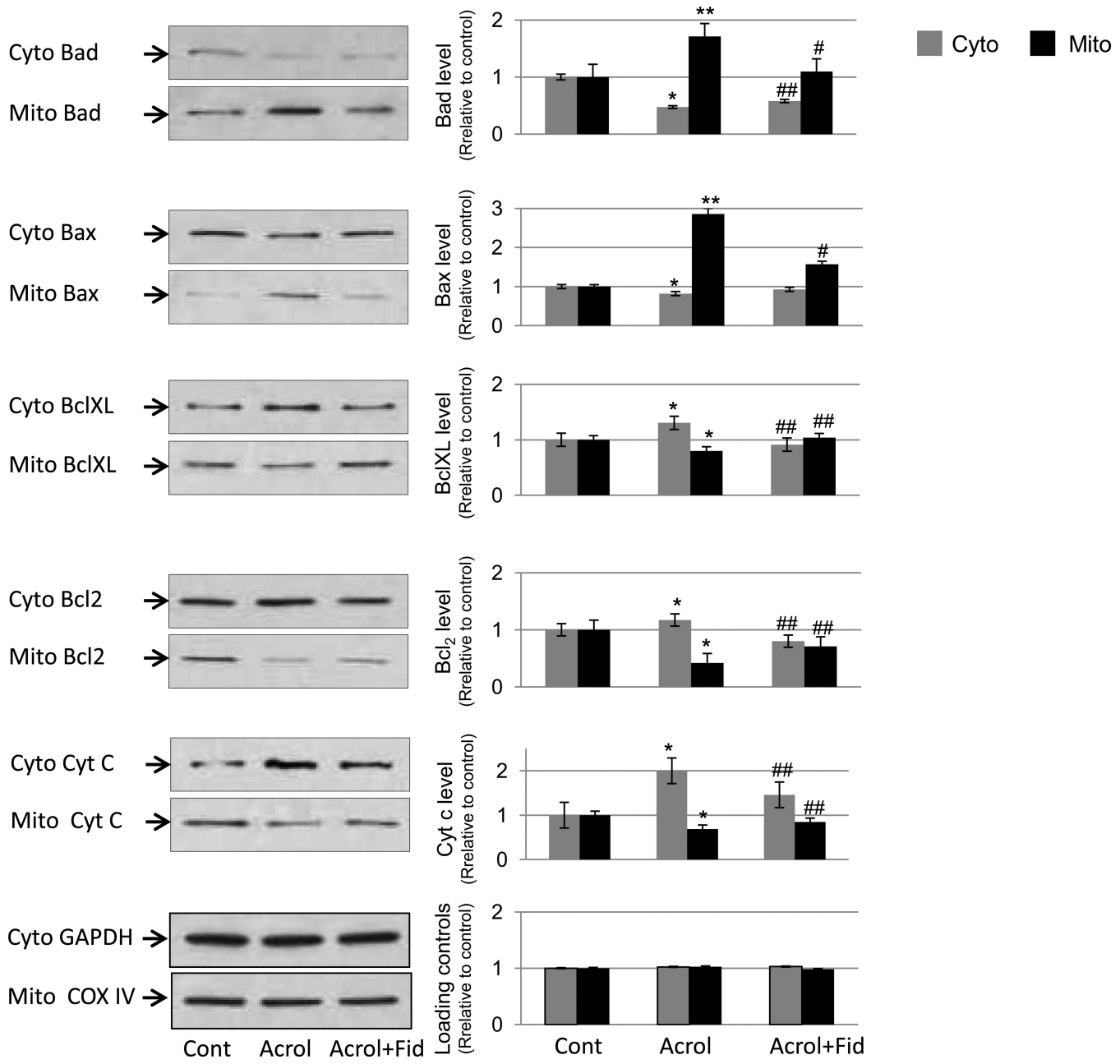

Fig 3. AR inhibition in airway epithelial cells prevents acrolein-induced translocation of Bcl2 family proteins

Approximately 80% confluent SAECs in T-75 flasks were incubated with or without fidarestat (10 μM) for 24 h. The cells were incubated with acrolein (5 μM) for 3 h after which cytosolic and mitochondrial fractions were prepared and Bcl_2 member proteins and cytochrome c were detected using specific antibodies by immunoblotting. A representative blot from duplicate experiments is shown in the left column. The right column shows densitometric analyses of respective protein bands relative to the untreated control. *p< 0.01 Vs Control; **p<0.001 Va Control; $^{\#}p$<0.01 Vs Acrolein' $^{\#\#}p$<0.05 vs acrolein. Cont, control; Acrol, acrolein; Fid, fidarestat

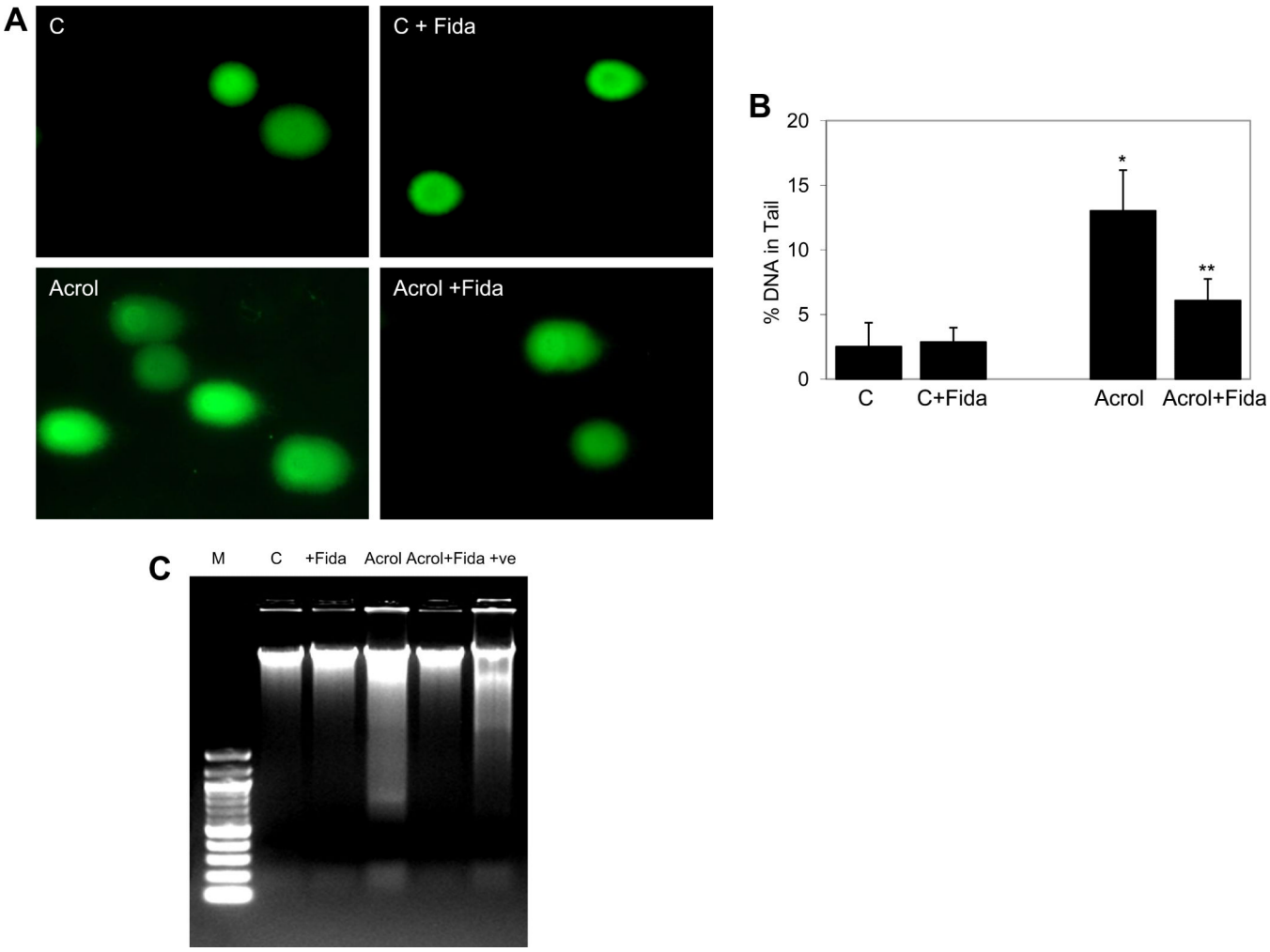

Fig 4. Effect of AR inhibition on Acrolein-induced DNA damage in SAEC

(A) Approximately 2×10^5 SAECs were seeded in a 6-well plate, and starved in 0.1% serum medium without or with fidarestat (10 μM) for 18 h. The cells were washed with HBSS and stimulated with acrolein (5μM) for 3h and comet assay was performed. The representative comets photomicrographs are shown (n=3). **(B)** Quantification of the comet is shown as bar diagram representing % DNA in comet tail (mean±SD) (*p<0.001 vs Control, **p<0.01 vs. Acrolein. **(C)** Approximately 75% confluent SAECs in T-75 flasks were starved overnight without or with fidarestat (10 μM) for 24 h, washed twice with HBSS and incubated with acrolein (5μM) for 18 h without or with fidarestat (10μM). The cells were harvested, washed with ice-cold PBS and DNA was extracted and 1 μg DNA was subjected to Agarose gel electrophoresis. UV-irradiated A549 cells-derived DNA was used as positive control. (n=3). C, control; Acrol, Acrolein; Fida, fidarestat.

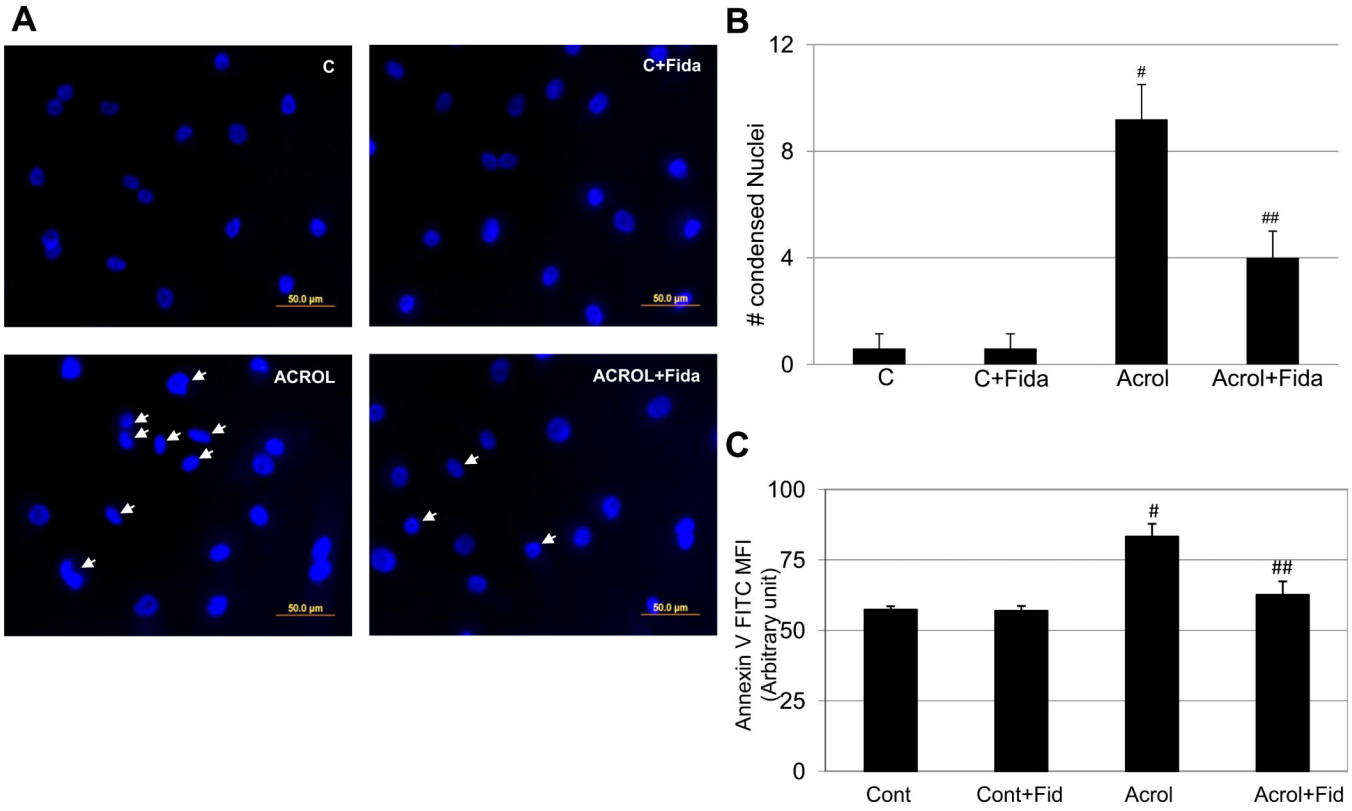

Fig 5. Effect of AR inhibition on acrolein-induced nuclear condensation and apoptosis in SAECs

(A) Approximately 75% confluent SAECs in 2-chambered slides were growth-arrested for 24h in 0.1% serum medium without or with AR inhibitor. The cells were washed with HBSS and stimulated with acrolein (5μM) for 24h. The cells were washed with cold PBS and mounted with DAPI containing mounting medium and observed with epifluorescence microscope and photographed. The representative photomicrographs are shown (n=3). **(B)** The quantification of the condensed nuclei was performed by manual counting per viewing area (5 areas per slide; four corners and center). An SEM±SD of three slides is presented as bar diagram. $^{\#}p<0.0001$ vs Control; $^{\#\#}p<0.002$ Vs Arolein. C, control; Acrol, Acrolein; Fida, fidarestat. **(C)** SAECs (10^5cell/well) were seeded and cultured till ~75% confluence. The cells were starved with or without fidarestat (10 μM) for 24 h and incubated with acrolein for 8 h and stained with Annexin V FITC. The mean fluorescence intensities (excitation at 485, emission at 535nm) are presented as bars. Data represents SEM±SD (n=3) from different experimental groups. $^{\#}p<0.006$ Vs Control; $^{\#\#}p<0.03$ Vs Acrolein. Cont, Control; Fid, fidarestat; Acrol, acrolein

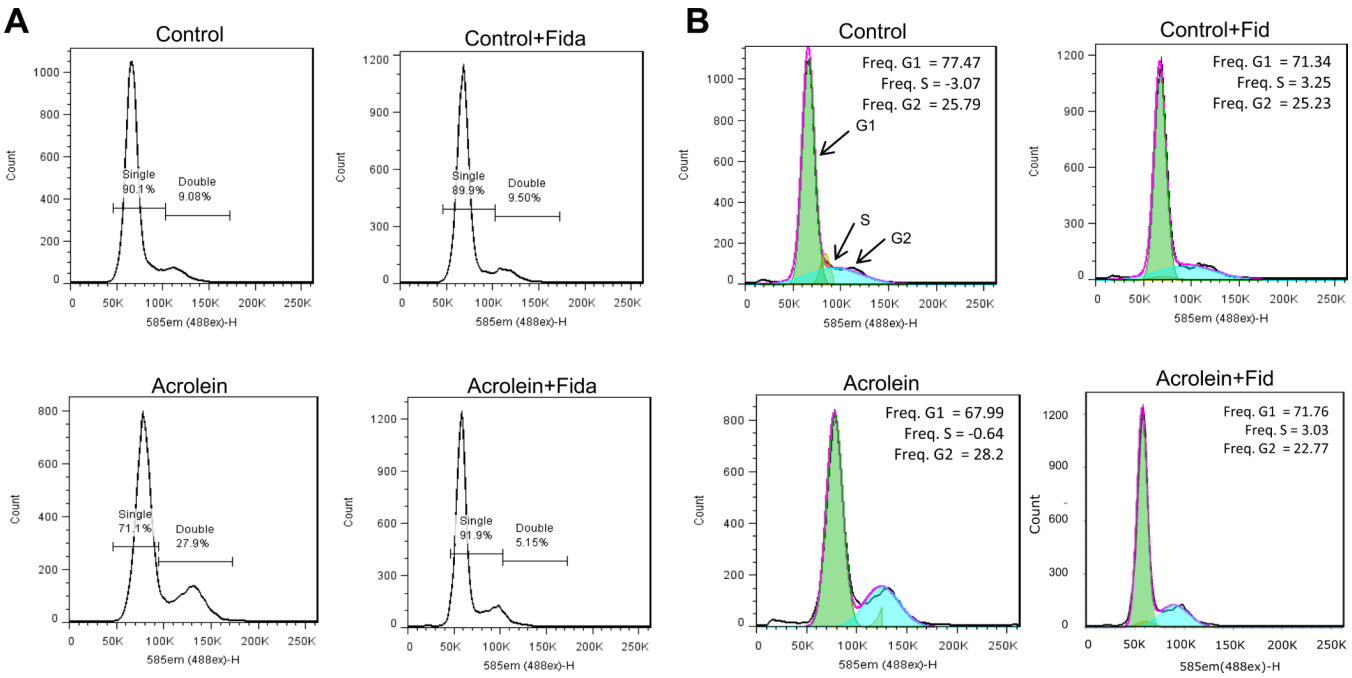

Fig 6. Effect of AR inhibition on acrolein-induced cell cycle arrest in SAECs

Approximately 75% confluent SAECs were growth-arrested and made quiescent by incubating in 0.1% serum medium without or with fidarestat for 24 h. The cells were rinsed with HBSS and incubated with acrolein (5μM) for 24 h. The cells were harvested and cycle analysis was performed by flow cytometry, and data is presented as histograms showing **(A)** percent nuclei with single and double set DNA, and **(B)** number of cells in different cell cycle stages (n=4). Fida, fidarestat.

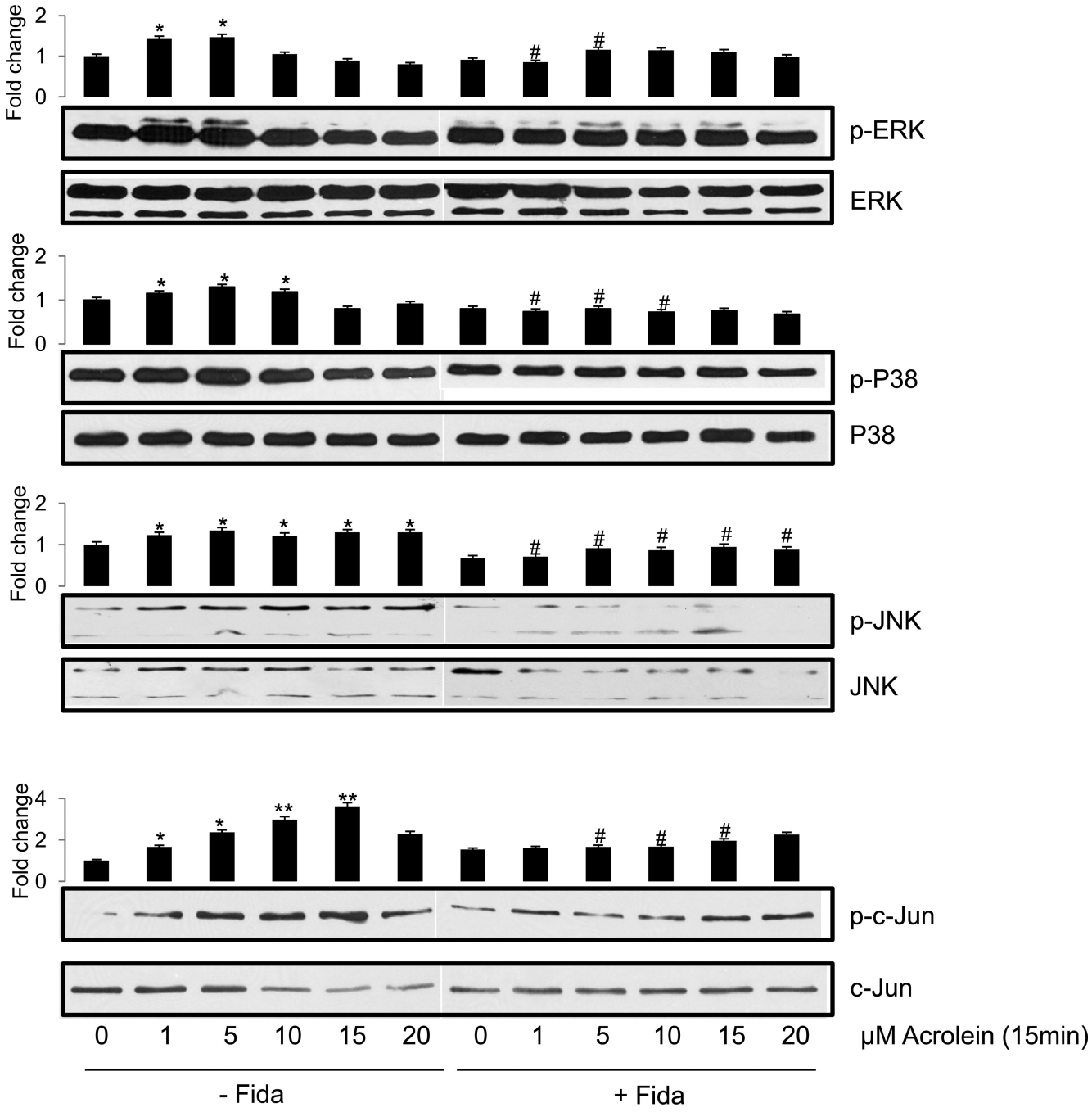

Fig 7. AR inhibition prevents acrolein-induced dose-dependent changes in phosphorylation of signaling intermediates in SAECs

Approximately 2×10^5 SAECs were seeded in 6-well plates, and growth arrested in 0.1% serum medium without or with fidarestat (10μM) for 24h. The cells were washed with HBSS and stimulated with acrolein for 15 min using different concentrations as indicated. Western blot analysis was performed using equal amount of proteins from each group, the representative blots are shown (n=3). The bars on the top of each blot show the fold-change in the pixel density of respective bands compared to control. *p<0.05 Vs control (0 μM acrolein); **p<0.01 Vs control (0 μM acrolein); $^{\#}p$<0.05 Vs acrolein-treated (corresponding concentrations); Fida, fidarestat

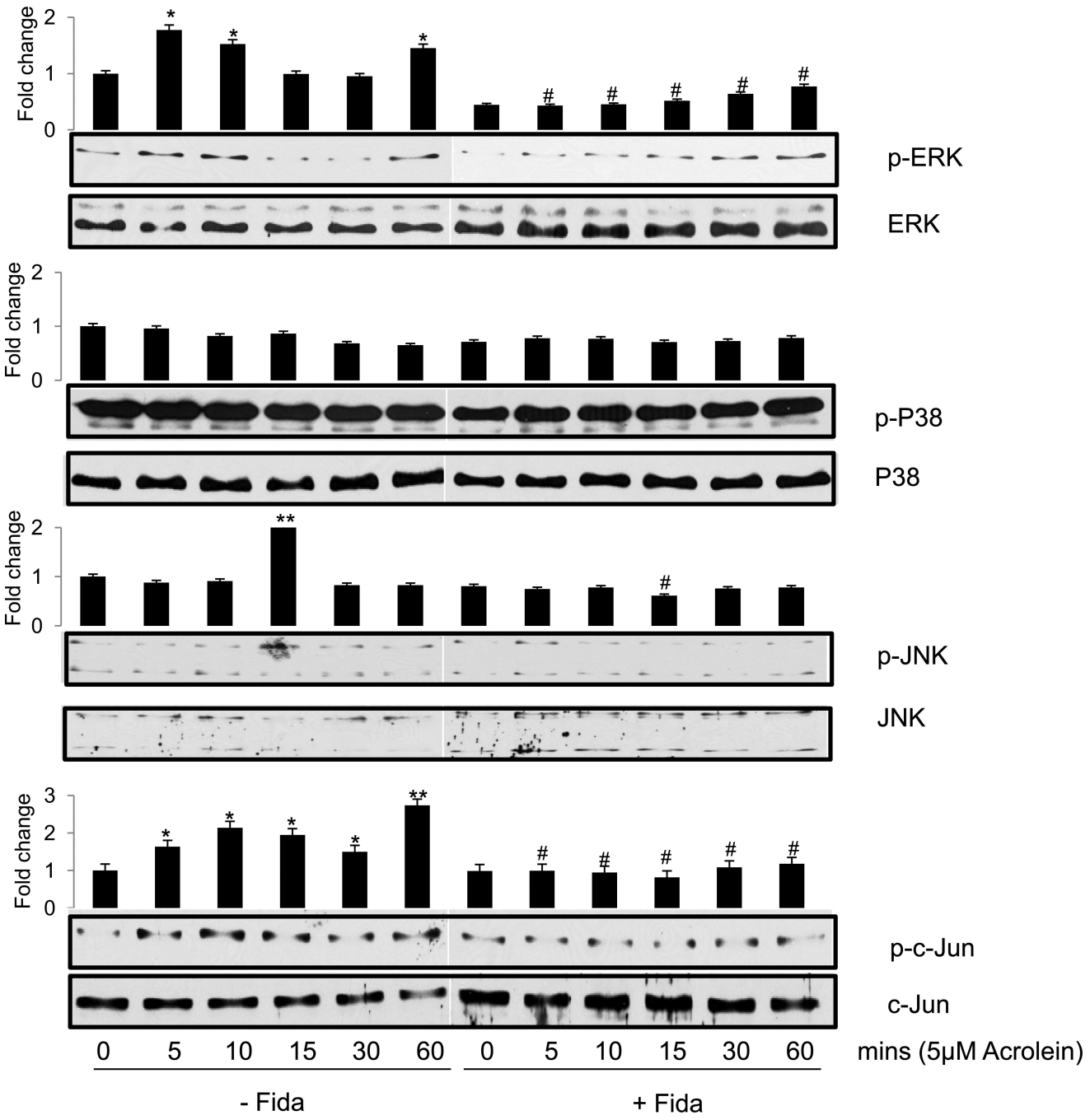

Fig 8. Effect of AR inhibition on Acrolein-induced time-dependent changes in the phosphorylation of signaling intermediates in SAECs

Approximately 2×10^5 SAECs were seeded in 6-well plates, and growth arrested in 0.1% serum medium without or with fidarestat (10μM) for 24 h. The cells were washed with HBSS and stimulated with acrolein (5μM) for different time intervals as indicated. Western blot analysis was performed using equal amount of proteins from each group, the representative blots are shown (n=3). The bars on the top of each blot show the fold-change in the pixel density of respective bands compared to control. *p<0.05 Vs control (0 μM acrolein); **p<0.01 Vs control (0 μM acrolein); $^{\#}p$<0.05 Vs acrolein-treated (corresponding time-points); Fida, fidarestat

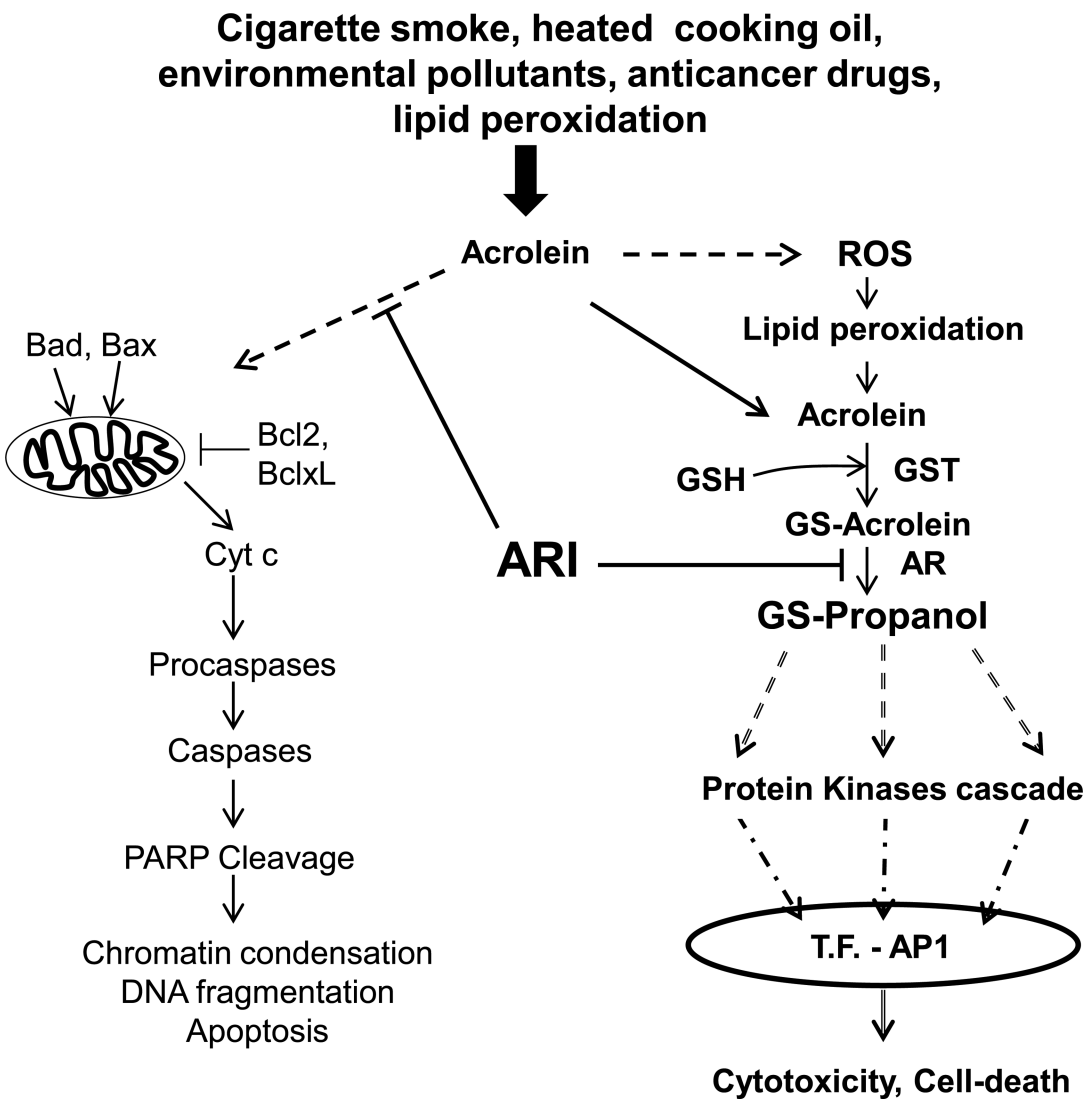

Fig 9. Schematic of mechanism of acrolein-induced apoptotic changes in airway cells and role of AR inhibition

Acrolein causes apoptosis by activating mitochondrial pathway of apoptosis by inducing the translocation of Bad and Bax to mitochondria and that of Bcl2 and BclXL to the cytosol and subsequent release of proapoptosis molecules causing caspase and PARP cleavage leading to apoptosis. Acrolein also increases ROS formation which via lipid peroxidation produces more of this reactive aldehyde, which in turn conjugates with cellular glutathione (GSH). The resultant conjugate is reduced by AR to GS-propanol, which activates stress kinases resulting in the activation of transcription factor (T.F.) AP-1. AP-1 transcribes inflammatory cytokines and chemokines genes causing cytotoxicity. Inhibition of AR blocks these changes at various levels as indicated by blunt arrows.